Proc. Natl. Acad. Sci. USA
Vol. 87, pp. 5528–5532, July 1990
Biochemistry

Mode of interaction of the zinc finger protein TFIIIA with a 5S RNA gene of *Xenopus*

(footprinting/hydroxyl radical)

MAIR E. A. CHURCHILL*, THOMAS D. TULLIUS†, AND AARON KLUG*

*Medical Research Council Laboratory of Molecular Biology, Hills Road, Cambridge CB2 2QH, England; and †Department of Chemistry, The Johns Hopkins University, Baltimore, MD 21218

Contributed by Aaron Klug, April 27, 1990

ABSTRACT **The zinc finger protein TFIIIA, a positive transcription factor of the 5S RNA gene, binds to an internal control region of 50 nucleotides. Two modes of binding have been considered for the TFIIIA–DNA complex, one of which has been proposed on the basis of nuclease and chemical protection experiments and the other on model building. Since then, evidence has accumulated on the structures of individual components of the complex—for example, zinc finger polypeptides studied by NMR and a segment of the binding site analyzed by x-ray crystallography, but no high-resolution structural data on the TFIIIA–DNA complex itself are available. Probes used previously to study the TFIIIA–DNA complex do not react with every nucleotide of DNA, unlike hydroxyl radical, which cleaves DNA at every backbone position. We describe here the quantitative analysis of high-resolution hydroxyl radical footprints and suggest how the array of zinc fingers might interact with the double helix.**

Transcription factor IIIA (TFIIIA) is the archetype of a class of proteins that use the zinc finger motif for DNA binding (1–3). No complexes of zinc finger proteins with DNA have so far yielded to structural analysis, so we must rely on mutagenesis (4–6), chemical and nuclease probing in solution (7–9), and model building (10, 11) to suggest how binding might occur. The nine zinc fingers of TFIIIA bind to ≈50 base pairs (bp) of the internal control region of the 5S ribosomal RNA gene of *Xenopus* (12–14). DNase I (6, 15) and hydroxyl radical (15) footprints of TFIIIA deletion mutants on the 5S RNA gene show that TFIIIA protects the internal control region in a collinear fashion. Two models for the TFIIIA–DNA interaction have been considered (9): (*i*) the "wrapping around" model, where successive zinc fingers make structurally equivalent contacts in the major groove without crossing over the minor groove (10), and (*ii*) the "alternating" model, where alternate fingers bind on one face of the DNA in an equivalent manner to the major groove, so that successive minor grooves must be crossed (9). Protection experiments that use DNase I and DNase II (8), micrococcal nuclease, and dimethyl sulfate (9) suggest that TFIIIA binds in the major groove, mainly to one face of the DNA helix and, therefore, support model *ii*. However, a model of the zinc finger polypeptide proposed by Berg (10), which agrees in its essentials with recent two-dimensional NMR structure determination (16, 17), has been considered to favor the "wrapping around" mode of binding to DNA. To help settle this question we have analyzed quantitatively hydroxyl radical footprints of the intact TFIIIA–DNA complex. We discuss the feasibility of the two models and propose a mode of binding consistent with the results from all of the studies on the TFIIIA–DNA complex.

The publication costs of this article were defrayed in part by page charge payment. This article must therefore be hereby marked "*advertisement*" in accordance with 18 U.S.C. §1734 solely to indicate this fact.

Quantitative Hydroxyl Radical Footprinting. Footprinting, i.e., protection against chemical or enzymatic attack, has been used to determine the DNA-binding sites of many drugs and proteins (18–20). The use of hydroxyl radical as the cleavage agent in footprinting experiments can reveal structural features of protein–DNA complexes that other probes do not detect (15, 21, 22). Two distinguishing characteristics of this technique are responsible for this higher resolution. Hydroxyl radical, which is generated by the reduction of hydrogen peroxide by iron(II) EDTA, is a small and very reactive species that abstracts a hydrogen atom from the deoxyribose, resulting in strand scission at the point of attack. The small size allows cleavage at every backbone position, making more structural information available, in principle, than other probes used so far, which do not sample the protection at every nucleotide. The second advantage of the hydroxyl radical lies in its low sequence-specificity, which arises because it does not bind to DNA and, moreover, does not compete with weakly bound protein. One disadvantage of the technique, however, is that the small size of the hydroxyl radical makes it relatively less sensitive than other probes to protection by proteins and to inhomogeneities in DNA structure, so that differences in the DNA-cleavage rate are often small and difficult to measure. To extract the subtle structural information available with such a small probe, quantitative analysis of the cleavage patterns is essential.

Hydroxyl radical footprints of TFIIIA and deletion mutants have been published, and the analysis and interpretation of those results allowed a detailed correlation of specific regions of the protein with regions of the DNA-binding site (15). However, footprints and subtraction plots from only one strand of the DNA were presented. In addition, the data were not analyzed quantitatively, so that the high-resolution features inherent in the data were not brought out and the nature of binding was not discussed. In this work we analyze hydroxyl radical footprints quantitatively and find these high-resolution details in the protection pattern. With these new results we can examine the two general models more critically and suggest a mode of binding for the TFIIIA–DNA complex that also considers the now-established structure of a zinc finger domain.

MATERIALS AND METHODS

Preparation and Hydroxyl Radical Footprinting of the TFIIIA–DNA Complex. The 183-bp *Eae* I–*Pvu* II fragment of plasmid pXbs1 was 5′ (noncoding strand) or 3′ (coding strand) end-labeled at the *Eae* I site and was combined with unlabeled *Hin*dIII–*Hpa* II fragment of pXbs1 (containing the 5S gene) in TFIIIA binding buffer [20 mM Hepes (pH 7.5)/70 mM KCl/7 mM $MgCl_2$/20 μM $ZnCl_2$/0.1% Nonidet P-40]. TFIIIA was obtained from 7S ribonucleoprotein particles (23). The particle was treated with RNase A (28.5 nM) solution and incubated with the DNA solution (9.5 nM in TFIIIA-binding site) at 22°C for 15 min, as described (15). The hydroxyl radical cleavage reagents were allowed to react with the DNA or DNA–TFIIIA

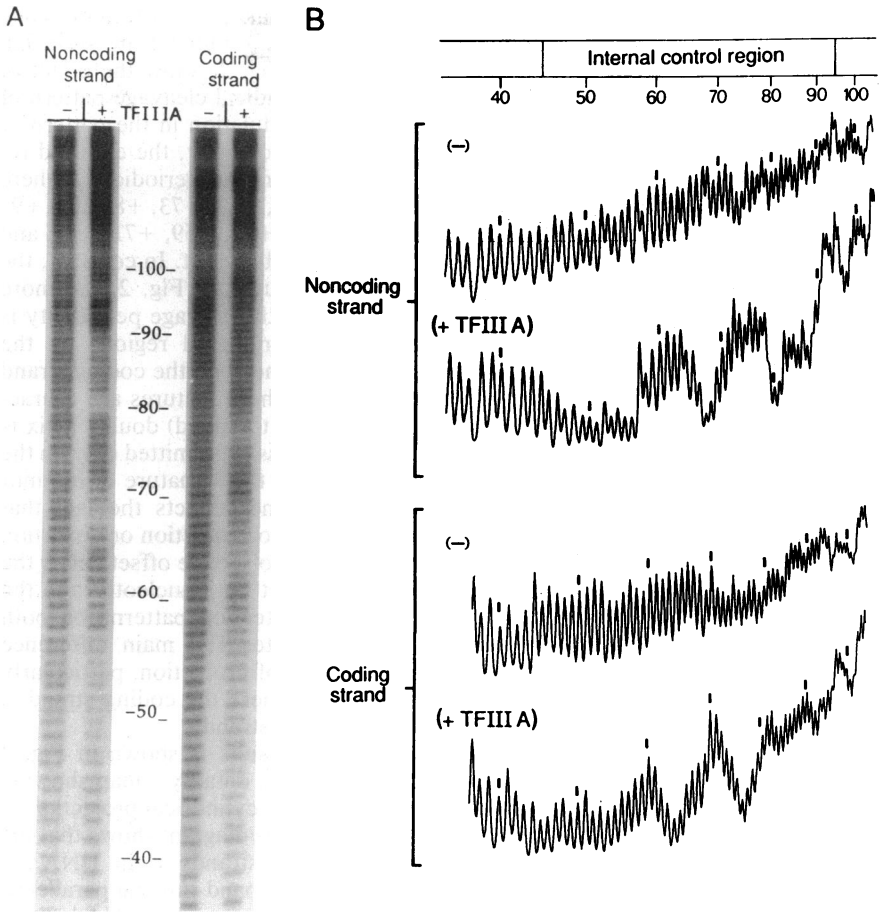

FIG. 1. Hydroxyl radical footprints of TFIIIA on the 5S gene of *Xenopus*. (*A*) A typical set of lanes from autoradiographs of TFIIIA footprinting experiments, showing the cleavage pattern of the noncoding and coding strands with and without TFIIIA. (*B*) Densitometer tracings showing the coding and noncoding strand with and without TFIIIA from the autoradiograph illustrated in *A*. A profile of each lane such as those shown here was obtained after a one-dimensional scan and background subtraction.

mixtures for 1 min at room temperature. Final concentrations of iron(II), EDTA, H_2O_2, and ascorbate in the solutions were 100 μM, 200 μM, 0.003%, and 1 mM, respectively. The hydroxyl radical cleavage reaction in the protein–DNA mixtures was stopped by the addition of a 10% (vol/vol) glycerol loading buffer (0.5× TB, without dyes; 1× TB is 89 mM Tris/89 mM borate) and then was loaded onto a 6% (0.5× TB; 30:1 acrylamide/bisacrylamide) polyacrylamide bandshift gel in 0.5× TB running buffer. The DNA in the shifted band was recovered from the gel. The other samples were quenched, as described previously. All samples were precipitated, rinsed with 70% ethanol, dried, redissolved in water, and quantitated by scintillation counting. The samples were then dried, redissolved in formamide/dye loading buffer, and heated at 90°C for 1 min before electrophoresis. They were loaded at intervals onto a 8% denaturing polyacrylamide gel (preelectrophoresed so that the gel temperature was between 43°C and 46°C), which was electrophoresed for 4 to 5 hr at 50–60 W constant power. The gel was dried and exposed to preflashed XAR-5 film (Kodak) at room temperature without an intensifying screen.

Quantitative Analysis of Hydroxyl Radical Footprints. Digitized images were produced by scanning the autoradiographs by using a densitometer, custom-built in this laboratory (100-μm resolution in the long direction of the autoradiograph). A profile of each lane was obtained using the GELTRAK program (24), and the area of each band was determined. A peak-area determination method, which uses simple integration, provided raw peak areas for each cleavage site along the DNA fragment with and without TFIIIA. The cleavage frequency at each site was calculated from these raw peak areas using a modified version of the method of Lutter (25):

$$P_i = \mathrm{Int}_i/[F + (\mathrm{Int}_{av})(N - i)].$$

P_i is the probability of cleavage at site i, Int_i is the raw integral of site i. Int_{av} is the average integral of all scanned sites from the lane. F is the integral of the uncut DNA, approximated as $F = 4N(\mathrm{Int}_{av(\text{naked DNA})})$, where N is the length of the fragment and the value 4 assumes that there is roughly 75% uncut DNA, which based on past experience is a reliable estimate.

Each set of raw data consisted of the peak areas from samples that had been electrophoresed for three different lengths of time (on the same autoradiograph). A representative portion of an autoradiograph and the corresponding densitometer profiles are shown in Fig. 1. Difference probability plots were calculated by subtracting the ln P_i of the naked DNA lane from the ln P_i of sample lanes after scaling to zero at the ends of the binding site. The raw data were spliced together to give three final data sets. Plots in Fig. 2 are the means of these three final data sets for each strand, smoothed by a three-bond average.

This quantitation method can measure the protection patterns of ligands that cause as little as 15% decrease in intensity of the DNA-cleavage pattern. Ten to fifteen percent is a reasonable estimate of the experimental error accrued after reaction set-up, scintillation counting, and gel-loading. The estimates that were used here can lead to a systematic error of up to 10% when, for some reason, the lanes do not have the same cleavage rate.

RESULTS

Hydroxyl radical footprints of TFIIIA on both strands of the internal control region of the *Xenopus borealis* somatic 5S RNA gene are shown in Fig. 1*A* and densitometer tracings in Fig. 1*B*. Protection from hydroxyl radical cleavage is obvious in some parts of the footprint but is not so clear in other parts. On the coding strand the footprint extends from nucleotide

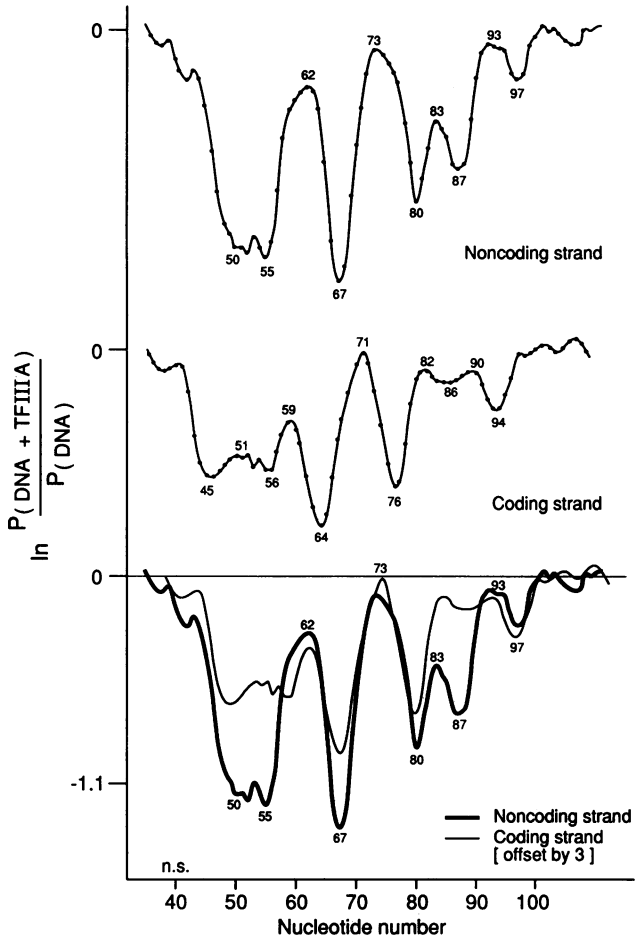

FIG. 2. Difference logarithm probability plots of hydroxyl radical footprints of TFIIIA on the noncoding and coding strands of the 5S gene. The plots shown are for the noncoding strand (top plot), coding strand (middle plot), and both strands overlaid with the pattern of the coding-strand offset from its true position by 3 nucleotides in the 3′ direction (bottom plot).

+40 (numbering from the start site of the gene) at the 5′ end of the internal control region to +96 at the 3′ end and from +42 to +98 on the noncoding strand. Exposed regions tend to occur regularly on both strands, but the details are difficult to visualize without quantitative analysis.

From the densitometer data we calculated the logarithm of the probability of cleavage at each site of the DNA–TFIIIA complex and subtracted the logarithm probability of cleavage at each corresponding site of the naked DNA (the rationale for this is explained in refs. 9 and 25). Plots of the logarithm difference probability values, in Fig. 2, show the effect of TFIIIA binding on the hydroxyl radical cleavage pattern of both strands. There is a clear modulation in the pattern of exposure to hydroxyl radical. Specifically, the exposed regions (peaks in Fig. 2) show a striking periodicity, where relatively exposed nucleotides +43, +62, +73, +83, and +93 on the noncoding strand and +41, +51, +59, +71, +82, and +90 on the coding strand are ≈10 bp apart. In contrast, the regions protected by TFIIIA (troughs in Fig. 2) are more irregular in length and depth, but the average periodicity is also 10–11 bp. Moreover, the protected regions on the noncoding strand are offset from those on the coding strand by 3 bp in the 3′ direction. Both these features are characteristic of a situation where a (right-handed) double helix is protected on one face, so that access is permitted only on the other face (26). This offset is also the signature of a minor groove interaction (20, 25, 27) and reflects the fact that hydroxyl radical is most sensitive to protection or distortion of the minor groove of the DNA. To see the offset better the plots have been overlaid and offset by 3 nucleotides in the lower portion of Fig. 2. The protection patterns on both strands are now seen to correlate. The main difference between the strands is the degree of protection, particularly at the ends of the binding site, where the coding strand is more exposed than the noncoding strand.

A better impression of these results is shown in Fig. 3 where we represent the quantitative data by a map showing levels of protection by TFIIIA on a cylindrical projection of the idealized DNA-binding site. This diagram shows that the most frequently cut bonds on both strands of the DNA are concentrated in a relatively narrow band running parallel to the helix axis and, hence, that one face of the DNA helix is exposed to hydroxyl radical cleavage. In fact, the whole binding site on this face is relatively exposed, except for bases +50 to +54 on the noncoding strand.

DISCUSSION

A change in the pattern of cleavage by hydroxyl radical can be due to direct protection by the protein, local distortion of the DNA by the protein, or even global distortions, such as bending induced by the protein, and, therefore, we cannot be quite certain of the origin of every change in the protection pattern. Nevertheless, the protection pattern in Fig. 3 considered as a whole indicates very strongly how the TFIIIA protein is arranged relative to the DNA-binding site. There are nine fingers in TFIIIA, so that, despite the irregularities

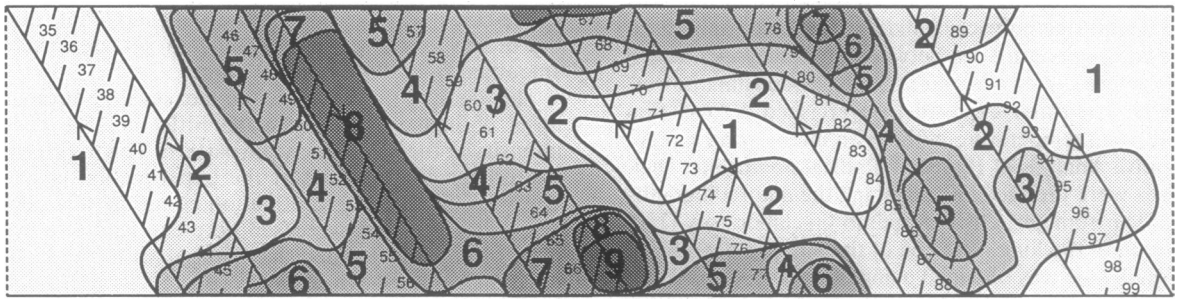

FIG. 3. Map of protection and exposure to hydroxyl radical for the TFIIIA–5S gene complex. Difference logarithm probability values corresponding to exposure at every site on each strand of the TFIIIA binding site were read from Fig. 2 for each position in the binding site and mapped onto a cylindrical projection of an idealized DNA helix that has a helical periodicity of 10.7 bp per turn (28). Contours were drawn and levels labeled 1–9 in an increasing scale of protection and shaded accordingly so that the most exposed regions appear the lightest. The small numbers shown on the minor groove of the DNA denote nucleotide positions. Note that this cylindrical projection has been produced by slitting the cylinder along the helix axis opposite to the exposed face of the DNA. To see the protected region more clearly, the cylinder can be slit along the exposed face (in the middle) and rejoined so that the protected face is now continuous and the exposed face is cut into two parts located at the top and bottom edge of the new diagram.

in the protection pattern, the general nature of the interaction emerges clearly. With fewer fingers the overall pattern might not have been evident because of the larger relative effect of local variations in the protection pattern. In any case, we would not expect to find a perfect 10- or 11-fold modulation in the protection pattern because the interaction of DNA with a complex protein having nine domains that differ in essential local details will not have the simplicity of a DNA duplex bound to an atomically flat surface (29). Despite the variations in exact positions and heights of individual peaks in the protection pattern, an overall 10- to 11-bp periodicity is evident over the length of the TFIIIA–DNA complex.

Thus, the hydroxyl radical footprinting data provide support for the alternating model *ii* of Fairall, Rhodes, and Klug, in which one face of the DNA is exposed (8, 9). To explain the data in terms of the wrapping-around model would require that the DNA be distorted by the protein roughly every 10 bp by fingers that bind, on average, every 5 bp (9, 15)—i.e., alternate fingers would still need to interact differently with the DNA. This situation is most unlikely and, moreover, the length of the linker (see below) poses a limitation on the length of the binding site that can be covered by this type of model (11). Another formal possibility is that the 10-bp periodic pattern could result from DNA bending (30), but this would have to be achieved by zinc fingers wrapping around the DNA in the major groove at positions rotated ≈90° from the plane of the bend, which is difficult to envisage.

How can we reconcile these protection data with the actual structure of a zinc finger? Miller *et al.* (1) suggested that TFIIIA is made up of discrete domains ≈30 amino acids long, in which each domain folds around a zinc ion and an invariant hydrophobic core. The first three-dimensional model for the zinc finger was proposed by Berg (10), based on these considerations and the structures of other metalloproteins. The N terminus forms an anti-parallel β-sheet and a reverse-turn from which the two cysteines bind to the zinc ion, whereas the C-terminal residues form an α-helix from which the histidines also bind the zinc. The entry and exit points of the polypeptide chain predicted in this model are located at opposite ends of the domain, which has been taken to imply a simple continuity between fingers, thus favoring the wrapping around model with its equivalent linkers (10). Recently Wright and coworkers (17) have solved the structure of a zinc finger by using two-dimensional NMR. The structure confirms the essential elements of the Berg model, although a few details are different. The actual length of the proposed β-sheet is unknown, and it may not continue to the very end of the finger (cf. Fig. 4 *Inset*). We take the N terminus of the finger *per se* and, therefore, the boundary of the linker to be at the invariant tyrosine/phenylalanine (Y/F), which is two amino acids away from the first cysteine of a finger. This Y/F has recently been shown by two-dimensional NMR to be part of the hydrophobic core of the finger (31). This disposition of the ends of the domain permits us to suggest a mode of connection between the fingers that can reconcile the experimental data on the TFIIIA–DNA complex with the structure of a single domain.

A Mode of Interaction of TFIIIA with Its DNA-Binding Site. The mode of binding illustrated in Fig. 4 takes into account the zinc finger structure, the combined earlier protection data (9), and the key features of the hydroxyl radical footprints presented here, such as the general 10-bp periodicity and asymmetric protection of the two strands. The figure shows zinc fingers in the major groove, all with the same polarity (although not necessarily the same specific orientation) but with linkers alternately located in the major groove or crossing over the minor groove. The protein as a whole lies on one face of the DNA, thus exposing the opposite face, for example, at positions +41, +51, +59, +71, +82, and +90 on the coding strand. The entry and exit points of the linker polypeptide are in positions where both crossing over the minor groove and connections within the same major groove are possible.

Inspection of models shows that the linkers would seem long enough to cross over the minor groove where required. An estimate of the distance to be spanned by a linker crossing the minor groove is ≈15 Å, and the length of an extended chain of five amino acids, the average linker is ≈18 Å (28). Crossing over a minor groove would also require a change in the direction of the linker, so it is highly relevant that the linker sequences in zinc finger proteins often contain prolines (1) (in particular a proline often precedes the invariant tyrosine/phenylalanine two residues before the first cysteine of a finger) or other amino acid sequences that might cause or allow changes in linker direction. Because there are no structural data on the linker sequences, the precise interaction with the DNA remains unknown. The precise rotational orientation and inclination of the fingers in the grooves cannot be determined from footprinting data, but clearly certain orientations, one of which is illustrated schematically in Fig. 4, allow some models to be built more easily than others. Finally, our proposal is one for the general mode of binding of TFIIIA to DNA and does not necessarily explain the irregularities in the protection pattern from local varia-

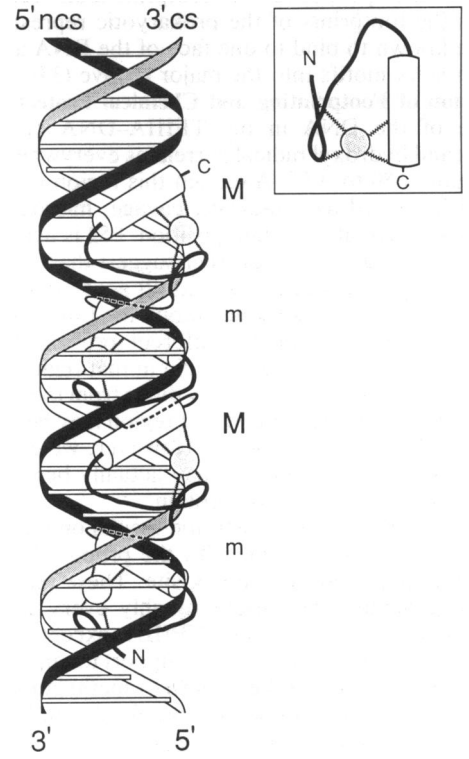

FIG. 4. Schematic diagram of zinc fingers placed on a DNA helix to show the mode of interaction favored by hydroxyl radical-protection data. The drawing of the zinc finger shown in the inset was adapted from the figure of Wright and coworkers that appeared on the cover of *Science* (ref. 17; copyright AAAS); the β-loop is on the left, and the helix on the right is represented by a cylinder. In the diagram of the "complex" the zinc fingers have been foreshortened to allow presentation to the DNA helix at appropriate angles. Protection is achieved on one face of the DNA simultaneously maintaining the same polarity for all the fingers. Successive fingers are connected alternately in the major groove M or by crossing over the minor groove m. The noncoding strand (ncs) is drawn in black, and the coding strand (cs) is drawn in grey. Linkers are drawn in a thinner line than the fingers and are dotted when they lie behind other objects in the diagram. This figure is not intended to describe the actual location or precise orientation of the zinc fingers in the binding site because the data, at present, cannot settle such detailed questions.

tions within the protein and DNA, although some of these variations do correlate with features in the protein and DNA.

We examined the protein sequence of TFIIIA (32) for a pattern of alternation to support these ideas. Although there is not an obvious pattern of alternation in the linker sequences, there is a slight alternation in the finger sequences themselves, where fingers 1, 3, 5, 7, and 9 have slightly more basic residues in their C-terminal halves than fingers 2, 4, 6, and 8. The sequence and length of the linkers between zinc fingers also correlate with certain features of the footprint. From previous footprinting experiments we know the relative polarity of the protein to the DNA sequence and the approximate locations of a few of the fingers (6, 15). The fingers that are linked by longer amino acid sequences, often containing Thr-Gly-Glu-Lys or related sequences, appear in the broad regions (+45 to +58) of the footprint shown in Fig. 2, whereas short linkers or those lacking this type of sequence occur in the middle fingers 4–7. The length of the linker sequence of fingers 5 and 6 is shorter than average, which correlates with the location of fingers 4–7 in the center of the footprint (15). In this central region (+60 to +82) the 10-bp variation in accessibility is very marked, suggesting that the protein is not reaching as deeply into the major groove as elsewhere. In fact, the central portion of the footprint looks remarkably similar to the footprints of the prokaryotic repressors (27), which are known to bind to one face of the DNA and direct helix-turn-helix motifs into the major groove (33).

Discussion of Footprinting and Chemical Protection Data. Exposure of the DNA in the TFIIIA–DNA complex to nucleases and hydroxyl radical correlates everywhere except in the region +50 to +55. Although this region is relatively protected from hydroxyl radical cleavage, micrococcal nuclease does cleave at +53, and position +52 is accessible to dimethyl sulfate (9), which together suggest that at least part of the phosphate backbone and a base is accessible there (cf. ref. 34). There are a few explanations for this discrepancy between the results from the different probes. The local protection of the DNA by the protein in that region (finger 9 and part of C-terminal domain) may differ from the rest of the protein or the DNA structure in that region may be altered in a special way by protein binding. However, we cannot rule out the possibility that finger 9 may actually behave differently than other fingers in the protein.

Earlier dimethyl sulfate protection results on the TFIIIA–DNA complex are consistent with the proposed setting of TFIIIA zinc fingers in the binding site. These results show that while guanines are present roughly every 5 bp, only every second set is protected by TFIIIA, except for +84 to +86 (see below), and hence provide support for an alternating model (9). At +84 to +86 the pattern of methylation protection in the TFIIIA–DNA complex breaks down, but modulation in the hydroxyl radical cleavage pattern is still periodic, which suggests that some protein is present in the major groove throughout about a turn of DNA. Thus, in these two regions, 50–55 and 83–86, the uncertainty engendered by deviation from a periodic pattern, shown by one probe, is made up for by the other probe.

That an alternating pattern of protection against methylation occurs (35) in the complex of another zinc finger protein, Sp1, (36) with its binding sites has been pointed out previously (29). Moreover, DNase I footprinting shows that one face of the DNA is exposed (36), so that the situation is parallel to that in the case of TFIIIA. Therefore, it would seem that at least TFIIIA and Sp1 share the same mode of interaction as we have described here, but we cannot say at this stage how general this is for all zinc finger proteins of the Cys-Cys/His-His type. Consideration of the sequence periodicity in the DNA (29) and the alternation in methylation protection of these two proteins raises the possibility that the DNA might to some extent determine the mode of binding of the protein.

Conclusions. We have presented here further evidence for the general nature of the geometry of binding of TFIIIA to its cognate DNA. The diagram of Fig. 4 shows how the same type of interaction between fingers and the major groove of DNA can be preserved while alternate linker sequences cross over the minor groove. The diagram uses the actual structure of a zinc finger (17) and also provides an explanation for all the results of chemical and nuclease probing experiments.

We are grateful to L. Fairall and D. Rhodes for gifts of the 7S ribonucleoprotein particle as a source of TFIIIA, J. Smith for assistance with the gel-scanning programs, and K. Vrana and D. Brown for their contributions in the earlier phase of this work. We thank D. Rhodes, A. Travers, A. McLachlan, G. Jacobs, and L. Fairall for helpful discussions and comments on the manuscript. M.E.A.C. was supported by a postdoctoral fellowship from the American Cancer Society.

1. Miller, J., McLachlan, A. D. & Klug, A. (1985) *EMBO J.* **4**, 1609–1614.
2. Brown, R. S., Sanders, C. & Argos, S. (1985) *FEBS Lett.* **186**, 271–274.
3. Klug, A. & Rhodes, D. (1987) *Trends Biochem. Sci.* **12**, 464–469.
4. Sakonju, S., Brown, D. D., Engelke, D., Ng, S.-Y., Shastry, B. S. & Roeder, R. G. (1981) *Cell* **23**, 665–669.
5. Pieler, T., Appel, B., Oei, S. L., Mentzel, H. & Erdmann, V. A. (1985) *EMBO J.* **4**, 1847–1853.
6. Smith, D. R., Jackson, I. J. & Brown, D. D. (1984) *Cell* **37**, 645–652.
7. Sakonju, S. & Brown, D. D. (1982) *Cell* **31**, 395–405.
8. Rhodes, D. (1985) *EMBO J.* **4**, 3473–3482.
9. Fairall, L., Rhodes, D. & Klug, A. (1986) *J. Mol. Biol.* **192**, 577–591.
10. Berg, J. M. (1988) *Proc. Natl. Acad. Sci. USA* **85**, 99–102.
11. Gibson, T. J., Postma, J. P. M., Brown, R. S. & Argos, P. (1988) *Protein Eng.* **2**, 209–218.
12. Brown, D. D. (1984) *Cell* **37**, 359–365.
13. Sakonju, S., Bogenhagen, D. F. & Brown, D. D. (1980) *Cell* **19**, 13–25.
14. Bogenhagen, D. F., Sakonju, S. & Brown, D. D. (1980) *Cell* **19**, 27–35.
15. Vrana, K. E., Churchill, M. E. A., Tullius, T. D. & Brown, D. D. (1988) *Mol. Cell. Biol.* **8**, 1684–1696.
16. Parraga, G., Horvath, S. J., Eisen, A., Taylor, W. E., Hood, L., Young, E. T. & Klevit, R. E. (1988) *Science* **241**, 1489–1492.
17. Lee, M. S., Gippert, G. P., Soman, K. V., Case, D. A. & Wright, P. E. (1989) *Science* **245**, 635–637.
18. Tullius, T. D. (1989) *Annu. Rev. Biophys. Biophys. Chem.* **18**, 213–237.
19. Rhodes, D. (1989) in *Protein Function: A Practical Approach*, ed. Creighton, T. E. (IRL, Oxford), pp. 177–198.
20. Van Dyke, M. W., Hertzberg, R. P. & Dervan, P. B. (1982) *Proc. Natl. Acad. Sci. USA* **79**, 5470–5474.
21. Tullius, T. D., Dombroski, B. A., Churchill, M. E. A. & Kam, L. (1987) *Methods Enzymol.* **155**, 537–558.
22. Churchill, M. E. A., Tullius, T. D., Kallenbach, N. R. & Seeman, N. C. (1988) *Proc. Natl. Acad. Sci. USA* **85**, 4653–4656.
23. Miller, J., Fairall, L. & Rhodes, D. (1989) *Nucleic Acids Res.* **17**, 9185–9192.
24. Smith, J. M. & Thomas, D. J. (1990) *Comput. Appl. Biosci.*, in press.
25. Lutter, L. C. (1978) *J. Mol. Biol.* **124**, 391–420.
26. Rhodes, D. & Klug, A. (1980) *Nature (London)* **286**, 573–578.
27. Tullius, T. D. & Dombroski, B. A. (1986) *Proc. Natl. Acad. Sci. USA* **83**, 5469–5473.
28. McCall, M., Brown, T., Hunter, W. N. & Kennard, O. (1986) *Nature (London)* **322**, 661–664.
29. Rhodes, D. & Klug, A. (1986) *Cell* **46**, 123–132.
30. Schroth, G. P., Cook, G. R., Bradbury, E. M. & Gottesfeld, J. M. (1989) *Nature (London)* **340**, 487–488.
31. Neuhaus, D., Nakaseko, Y., Nagai, K. & Klug, A. (1990) *FEBS Lett.* **262**, 179–184.
32. Ginsberg, A. M., King, B. O. & Roeder, R. G. (1984) *Cell* **39**, 479–489.
33. Brennan, R. G. & Matthews, B. W. (1989) *J. Biol. Chem.* **264**, 1903–1906.
34. Drew, H. (1984) *J. Mol. Biol.* **176**, 535–557.
35. Gidoni, D., Dynan, W. S. & Tjian, R. (1984) *Nature (London)* **312**, 409–413.
36. Kadonaga, J. T., Carner, K. R., Masiarz, F. R. & Tjian, R. (1987) *Cell* **51**, 1079–1090.